HHS Public Access

Author manuscript

Nature. Author manuscript; available in PMC 2015 April 02.

Published in final edited form as:

Nature. 2014 October 2; 514(7520): 102–106. doi:10.1038/nature13596.

A long non-coding RNA protects the heart from pathological hypertrophy

Pei Han[1,6], **Wei Li**[#1], **Chiou-Hong Lin**[#1], **Jin Yang**[1,6], **Ching Shang**[1], **Sylvia T. Nuernberg**[1], **Kevin Kai Jin**[1], **Weihong Xu**[2], **Chieh-Yu Lin**[1], **Chien-Jung Lin**[1], **Yiqin Xiong**[1], **Huanchieh Chien**[1], **Bin Zhou**[4], **Euan Ashley**[1], **Daniel Bernstein**[3], **Peng-Sheng Chen**[6], **Huei-sheng Vincent Chen**[5], **Thomas Quertermous**[1], and **Ching-Pin Chang**[6,7,8,*]

[1]Division of Cardiovascular Medicine, Cardiovascular Institute, Stanford University School of Medicine, Stanford, CA 94305

[2]Stanford Genome Technology Center, Stanford University School of Medicine, Stanford, CA 94305

[3]Department of Pediatrics, Stanford University School of Medicine, Stanford, CA 94305

[4]Department of Genetics, Pediatrics, and Medicine (Cardiology), Albert Einstein College of Medicine of Yeshiva University, 1301 Morris Park Avenue, Price Center 420, Bronx, NY 10461

[5]Del E. Webb Neuroscience, Aging & Stem Cell Research Center, Sanford/Burnham Medical Research Institute, La Jolla, California 92037

[6]Krannert Institute of Cardiology and Division of Cardiology, Department of Medicine,

[7]Department of Biochemistry and Molecular Biology,

[8]Department of Medical and Molecular Genetics, Indiana University School of Medicine, Indianapolis, IN 46202, USA

[#] These authors contributed equally to this work.

Summary

The role of long noncoding RNA (lncRNA) in adult hearts is unknown; also unclear is how lncRNA modulates nucleosome remodeling. An estimated 70% of mouse genes undergo antisense transcription[1], including myosin heavy chain 7 (*Myh7*) that encodes molecular motor proteins for heart contraction[2]. Here, we identify a cluster of lncRNA transcripts from *Myh*7 loci and show a

[*]Author for correspondence: Ching-Pin Chang, M.D., Ph.D., Associate Professor of Medicine, 1800 N. Capitol Ave, E400, Indianapolis, IN 46202, changcp@iu.edu, Office: 317-274-0940, Fax: 317-962-0071 .

Author Contributions

C-P.C. and P.H. were responsible for the original concepts, design, and manuscript preparation. W.L. and C-H.L. contributed equally to the work. P. H. conducted most experiments; W.L. and J.Y. assisted with TAC, echo and reporter analyses; C-H. L protein purification; S.T.N ribosome data analysis; K.K.J. protein sequence and motif analysis; C.S. western blot studies; W.X. CSF scoring; Y.X. RNA/protein staining; C-J./C-Y. L. *Brg1*-null tissue preparation and H-10 antibody-ChIP optimization; H-C.C. cloning; HS.V.C. tissue collection; E.A. tissue collection/rat tissue supply; B.Z. driver line generation; D.B, P-S.C., and T.Q. data analysis.

Author Information

The authors declare no competing financial interests.

new lncRNA–chromatin mechanism for heart failure. In mice, these transcripts, which we named Myosin Heavy Chain Associated RNA Transcripts (*MyHEART* or *Mhrt*), are cardiac-specific and abundant in adult hearts. Pathological stress activates the Brg1-Hdac-Parp chromatin repressor complex[3] to inhibit *Mhrt* transcription in the heart. Such stress-induced *Mhrt* repression is essential for cardiomyopathy to develop: restoring *Mhrt* to the pre-stress level protects the heart from hypertrophy and failure. *Mhrt* antagonizes the function of Brg1, a chromatin-remodeling factor that is activated by stress to trigger aberrant gene expression and cardiac myopathy[3]. *Mhrt* prevents Brg1 from recognizing its genomic DNA targets, thus inhibiting chromatin targeting and gene regulation by Brg1. *Mhrt* binds to the helicase domain of Brg1, and this domain is crucial for tethering Brg1 to chromatinized DNA targets. Brg1 helicase has dual nucleic acid-binding specificities: it is capable of binding lncRNA (*Mhrt*) and chromatinized—but not naked—DNA. This dual-binding feature of helicase enables a competitive inhibition mechanism by which *Mhrt* sequesters Brg1 from its genomic DNA targets to prevent chromatin remodeling. A *Mhrt*-Brg1 feedback circuit is thus crucial for heart function. Human *MHRT* also originates from *MYH7* loci and is repressed in various types of myopathic hearts, suggesting a conserved lncRNA mechanism in human cardiomyopathy. Our studies identify the first cardioprotective lncRNA, define a new targeting mechanism for ATP-dependent chromatin-remodeling factors, and establish a new paradigm for lncRNA–chromatin interaction.

Keywords

lncRNA; *Mhrt*; Brg1; BAF; chromatin; gene regulation; myosin heavy chain; cardiomyocyte; cardiac hypertrophy; cardiomyopathy; heart failure

By 5′- and 3′-rapid amplification of cDNA ends, we discovered an alternative splicing of *Myh7* anti-sense transcription into a cluster of RNAs of 709 to 1147 nucleotides (*Mhrt*s), containing partial sequences of *Myh7* introns and exons (Fig. 1a, Supplementary information). *Mhrt*s were cardiac-specific (Fig. 1b), present at low levels in fetal hearts, with increasing abundance as the hearts matured and *Myh6*/*Myh7* increased (Fig. 1c). RNA *in situ* analysis showed that *Mhrt*s resided in the myocardium but not endocardium or epicardium (Fig. 1d, Extended Data Fig. 1a). Quantitation of nuclear/cytoplasmic RNA in heart extracts revealed that *Mhrt*s were primarily nuclear RNAs (Fig. 1e). Coding substitution frequencies[4,5] of *Mhrt*s predicted a negative/low protein-coding potential, *in vitro* translation of *Mhrt*s yielded no proteins, and ribosome profiling[6] revealed no/minimal ribosomes on *Mhrt* (Fig. 1f, Extended Data Fig. 1b–f, Supplementary text). Consequently, *Mhrt*s are non-coding RNAs in cardiomyocyte nuclei.

*Mhrt*s were down-regulated by 46–68% in hearts pressure-overloaded by transaortic constriction (TAC)[3], beginning by 2 days and lasting for ≥42 days after TAC (Fig. 2a). Such *Mhrt* reduction coincided with TAC-induced *Myh6*/*7* isoform switch characteristic of cardiomyopathy[7-9] (Extended Data Fig. 2a). To define *Mhrt* function, we focused on *Mhrt779*, the most abundant *Mhrt* species with 779 nucleotides (Fig. 2b and 2c, Extended Data Fig. 2b–e). We generated a transgenic mouse line to restore *Mhrt*779 level in stressed hearts. This transgenic line, driven by tetracycline response element (*Tre-Mhrt779*), was crossed to a cardiac-specific driver line (*Tnnt2-rtTA*)[3] that employs troponin promoter

(*Tnnt2*) to direct expression of reverse tetracycline-dependent transactivator (rtTA). The resulting *Tnnt2-rtTA*;*Tre-Mhrt779* line (abbreviated as *Tg779*) enabled the use of doxycycline to induce *Mhrt779* expression in cardiomyocytes. Within 7–14 days of doxycycline (dox) treatment, *Mhrt779* increased by ~1.5-fold in left ventricles of *Tg779* mice; this offset *Mhrt779* suppression in TAC-stressed hearts to maintain *Mhrt779* at pre-stress level (Fig. 2d). Six weeks after TAC, dox-treated control mice (*Tre-Mhrt779, Tnnt2-rtTA*, or wild-type) developed severe cardiac hypertrophy and fibrosis with left ventricular (LV) dilatation and reduced fractional shortening (FS). Conversely, dox-treated *Tg779* hearts—with *Mhrt779* maintained at pre-stress level—developed much less pathology, with 45.7% reduction of ventricle/body-weight ratio (Fig. 2e), 61.3% reduction of cardiomyocyte size (Fig. 2f, Extended Data Fig. 3a), minimal/absent cardiac fibrosis (Fig. 2g), 45.5% improvement of FS (Fig. 2h, Extended Data Fig. 3b), normalized LV size (Fig. 2i), and reduced pathological changes of *Anf, Bnp, Serca2, Tgfb1, and Opn* expression[10-13] (Extended Data Fig. 3c and 6e). To further test cardioprotective effects of *Mhrt*, we induced *Mhrt*779 after 1–2 weeks of TAC when hypertrophy had begun. This approach reduced hypertrophy by 23% and improved FS by 33% in 8 weeks after TAC (Extended Data Fig. 3d–f). The efficacy of late *Mhrt779* introduction suggests that a sustained repression of *Mhrt* in stressed hearts is essential for continued decline of cardiac function.

To study *Mhrt* regulation, we examined the 5′ upstream region of *Mhrts* (−2329 to +143) (Extended Data Fig. 4a) for signatures of lncRNA promoter: RNA Polymerase II (PolII), histone 3 tri-methylated lysine 4 (H3K4me3), and histone 3 tri-methylated lysine 36 (H3K36me3)[4,14,15]. By chromatin immunoprecipitation (ChIP) of left ventricles, we found that this putative promoter contained four evolutionarily conserved elements (a1 to a4)[3] that were enriched with PolII (a1 to a4), H3K4me3 (a1 and a4), and H3K36me3[14,16-18] (a1 and a3/a4) (Extended Data Fig. 4a–d). Conversely, no PolII, H3K4me3, or H3K36me3 enrichment was found in control *Shh* and *Vegfa* promoters or in thymus and lungs that did not express *Mhrts* (Extended Data Fig. 4b–d). These results reveal an active, cardiac-specific lncRNA promoter controlling *Mhrt* expression.

We then asked how *Mhrt* was repressed in stressed hearts. We postulated that cardiac stress activated Brg1 to occupy a1–a4 promoter to repress *Myh6*[3] and *Mhrt* in opposite transcription directions (Extended Data Fig. 4a). Indeed, *Mhrt* repression required Brg1: TAC suppressed *Mhrt*s in control but not *Brg1*-null hearts (*Tnnt2-rtTA;Tre-Cre;Brg1*$^{f/f}$)[3] (Extended Data Fig. 4e). To test Brg1 activity on *Mhrt* promoter, we cloned the a1-a4 promoter in *Mhrt* transcription direction (−2329 to +143) into an episomal luciferase reporter pRep4 that allows promoter chromatinization[19]. Brg1 was then transfected into Brg1-deficient SW13 cells[20] to reconstitute Brg1/BAF complex for reporter assays. Brg1 transfection caused ~50% reduction of *Mhrt* promoter activity ($p<0.0001$), and such *Mhrt* repression was virtually abolished by Hdac inhibition with trichostatin-A or Parp inhibition with PJ-34[21] (Extended Data Fig. 4f), indicating a cooperative repressor function between Brg1, Hdac, and Parp. ChIP verified that *Mhrt* promoter (a1-a4) was occupied by Brg1, Hdac2/9 and Parp1 in stressed hearts[3] and in pRep4 reporter episome (Extended Data Fig. 4g). These findings indicate that *Mhrt* is repressed by stress-induced Brg1–Hdac-Parp complex[3] through the a1–a4 promoter.

Because *Myh6* and *Mhrt* were both regulated by the a1–a4 promoter, we hypothesized that a1–a4 contained two elements to regulate *Myh6* and *Mhrt*—with a1 element controlling *Myh6* and a3/4 *Mhrt* (Extended Data Fig. 4a). On a1 and a3/4 (but not a2), we found cardiac-specific enrichment of Brg1[3], H3K4me3 and H3K36me3 (Extended Data Fig. 4c-d), and DNaseI genomic footprints (Fig. 3a)[22]. To test a3/4 for *Mhrt* regulation, we conducted deletional analysis of a1-a4 promoter in *Mhrt* transcription direction. In reporter assays, a3/4 was necessary and sufficient for *Mhrt* promoter activity and for Brg1-dependent *Mhrt* repression, whereas a1 was not essential for such controls (Extended Data Fig. 4h). Conversely, a1 is necessary and sufficient for Brg1 to repress *Myh6* promoter[3], but a3/4 is not required[3]. Therefore, a1 and a3/4 are two functionally distinct elements for Brg1 to separately control *Myh6* and *Mhrt*.

In stressed hearts Brg1 represses *Myh6* and activates *Myh7*[3], causing a pathological switch of *Myh6/7* expression, characteristic of cardiomyopathy[23]. Such stress/Brg1-dependent *Myh* switch was largely eliminated by *Mhrt779* (Fig. 3b), and the inhibition of *Myh* switch by *Mhrt* did not involve RNA-RNA sequence interference between *Mhrt* and *Myh* (Extended Data Fig. 5a-j, Supplementary text). Instead, it required physical interaction between *Mhrt* and Brg1. RNA immunoprecipitation of TAC-stressed adult hearts or Brg1-expressing neonatal hearts showed that Brg1 co-immunoprecipitated with *Mhrt779* but not control RNAs, and *Mhrt779* complexed with Brg1 but not polycomb Ezh2 or Suz2 (Fig. 3c, Extended Data Fig. 6a and 6b). The Brg1-*Mhrt* complex was minimal in unstressed adult hearts with low Brg1[3] or in stressed *Brg1*-null hearts (*Tnnt-rtTA;Tre-Cre;Brg1*$^{f/f}$)[3] (Fig. 3c, Supplementary text). These results suggest that *Mhrt* binds to Brg1 to influence its gene regulation.

We then tested how *Mhrt* regulated Brg1 activity on its *in vivo* target genes, including *Myh6*[3], *Myh7*[3], and *Opn* (Osteopontin, critical for cardiac fibrosis[12])(Extended Data Fig. 6c–e, Supplementary text). In dox-treated, TAC-stressed *Tg799* hearts, *Mhrt779*—without affecting Brg1 mRNA/protein level (Extended Data Fig. 7a-f)—reduced Brg1 occupancy on *Myh6*, *Myh7* and *Opn* promoters by 60–90% (Fig. 3d), causing a 56–76% loss of Brg1-controlled *Myh* switch and *Opn* activation (Fig. 3b, Extended Data Fig. 6e and 7g). We then used primary rat ventricular cardiomyocytes to conduct reporter assays. In these cells, as observed *in vivo*, Brg1 repressed *Myh6* and activated *Myh7* and *Opn* promoters; *Mhrt779* reduced Brg1 activity on these promoters by 54–80% (Fig. 3e). Accordingly, *Mhrt* prevents Brg1 from binding to its genomic targets to control gene expression.

How Brg1 or ATP-dependent chromatin remodelers recognize their target promoters is an important but not fully understood issue in chromatin biology. Biochemically, recombinant Brg1 proteins and *in vitro* transcribed *Mhrt779* could directly co-immunoprecipitate without involving other factors (Fig. 3f). Electrical mobility shift assay (EMSA) showed that Brg1 shifted biotin-labeled *Mhrt779* to form a low mobility protein–RNA complex that was competitively disrupted by unlabeled *Mhrt779* (Fig. 3f). Brg1, which belongs to SWI/SNF family of chromatin-remodeling factors, contains a helicase/ATPase core that is split by an insertion into two RecA-like domains: DExx-c (DEAD-like helicase superfamily c-terminal domain, D1) and HELIC-c (helicase superfamily c-terminal domain, D2)[24,25] with signature motifs of DEAD-box, superfamily 2 RNA helicase[25,26] (Fig. 3g, Extended Data Fig. 8).

SWI/SNF proteinş although conserved with RNA helicases, were observed to bind DNA[27] and mediate DNA structural changes and repair[19]. The binding properties of Brg1 remained undefined. To test if *Mhrt* could bind to Brg1 helicase, we generated MBP-tagged recombinant proteins that contained Brg1 DExx-c domain (MBP-D1, amino acid 774–913), HELIC-c domain with C-terminus extension (MBP-D2, 1086–1310), or entire helicase (MBP-D1D2, 774–1310)(Extended Data Fig. 9a). D1D2 showed the highest *Mhrt* binding affinity (K_d = 0.76 μM); D1 moderate (K_d = 1.8 μM); D2 modest (K_d > 150 μM)*;* MBP no binding (Fig. 3h and 3i). Therefore, Brg1 helicase binds *Mhrt* with high affinity.

Contrary to its potent RNA binding, Brg1 helicase had no detectable binding to the naked DNA of *Myh6* promoter (596bps, −426 to +170, critical for Brg1's control of *Myh6*[3]) (Extended Data Fig. 9b). To test if Brg1 helicase could bind chromatinized DNA, we generated nucleosomal DNA *in vitro* by assembling histone octamers (histone 2A, 2B, 3, and 4)[28] on *Myh6* promoter DNA, as well as on control *Neo* and 5SrDNA. We achieved 50–65% efficiency of nucleosome assembly, comparable among *Myh6*, *Neo*, and 5SrDNA (Fig. 4a). Because the large nucleosome size precluded a clear EMSA resolution, we used amylose to pull down MBP-tagged D1D2 proteins. We found that D1D2 pulled down nucleosomal *Myh6* promoter DNA but not the naked one (Fig. 4b). The pull-down efficiency of nucleosomal *Myh6* was ~3–6-fold that of *Neo* or 5SrDNA (Fig. 4c), and *Mhrt779* was capable of disrupting D1D2-*Myh6* pull-down (Fig. 4d). Although D1D2 bound to histone 3 (Fig. 4e), histone binding was insufficient to anchor D1D2 to nucleosomal DNA, as D1D2 bound poorly to nucleosomal *Neo* and 5SrDNA that also contained histones (Fig. 4c). Therefore, chromatinized DNA targets are biochemically recognized by Brg1 helicase, and this process is inhibited by *Mhrt*.

To test the ability of Brg1 to distinguish chromatinized from naked DNA promoters in cells, we cloned *Myh6* promoter into the luciferase reporter plasmid pREP4 (allowing promoter chromatinization[19]) and pGL3 (containing naked, non-chromatinized promoter). In rat ventricular cardiomyocytes and SW13 cells, ChIP and luciferase analyses showed that Brg1 bound and repressed chromatinized but not naked *Myh6* promoter (Fig. 4f and 4g, Extended Data Fig. 9c and 9d). However, without D1/D2 domain or in the presence of *Mhrt*, Brg1 was unable to bind or repress chromatinized *Myh6* promoter (Fig. 4h–j, Extended Data Fig. 9e), indicating the necessity of D1D2 for the interaction between Brg1, chromatin, and *Mhrt*. Consistently, all our genetic, biochemical, and cellular studies show that Brg1 requires the helicase domain to bind to chromatinized DNA targets, and *Mhrt* seizes the helicase to disrupt Brg1–chromatin binding.

We then asked how Brg1 surpassed its basal suppression by *Mhrt* to control *Myh*, *Mhrt*, *Opn*, or other genes to trigger cardiomyopathy (Supplementary text). Amylose pull-down experiments showed that Brg1 dose-dependently escaped from *Mhrt* inhibition to occupy *Mhrt* promoter (Extended Data Fig. 10). Brg1 protein, which increases under stress conditions[3], could therefore outrun *Mhrt* and gain control over *Mhrt* promoter to repress *Mhrt* expression and tip the balance toward Brg1. Contrary to the endogenous *Mhrt* that was repressible by Brg1, the *Mhrt* transgene (*Tg779*)—driven by *Tnnt2*/*Tre* promoters—was not subject to Brg1's repression and thus able to keep *Mhrt* at pre-stress level to inhibit Brg1

and reduce hypertrophy. This further demonstrates the necessity of *Mhrt* repression for myopathy to develop.

Human *MYH7* loci encoded RNA that resembled *Mhrt* in primary sequence and secondary structure predicted by minimal free energy[29] (Fig. 4k, Extended Data Fig. 11a and 11b). The human *MHRT* was also repressed in stressed hearts, with 82.8%, 72.8%, and 65.9% reduction of *MHRT* in hypertrophic, ischemic or idiopathic cardiomyopathy tissues (Fig. 4l, Extended Data Fig. 11c). This suggests a conserved *Mhrt* mechanism of human cardiomyopathy.

Discussion

Mhrt is the first example of lncRNA that inhibits myopathy and chromatin remodelers. Reciprocal *Mhrt*-Brg1 inhibition constitutes a negative feedback circuit critical for maintaining cardiac function (Fig. 4m). The helicase core of Brg1, combined with histone-binding domains of Brg1/BAF complex, adds a new layer of specificity control to Brg1/BAF targeting and chromatin remodeling (Fig. 4n). The *Mhrt*–helicase interaction also exemplifies a new mechanism by which lncRNA controls chromatin structure. To further elucidate chromatin regulation, it will be essential to define helicase domain function in all ATP-dependent chromatin-remodeling factors and to identify new members of lncRNA that act through this domain to control chromatin. The cardioprotective *Mhrt* may have translational value, given that RNA can be chemically modified and delivered as a therapeutic drug. This aspect of lncRNA–chromatin regulation may also inspire new therapies for human disease.

METHODS

Mice, animal sample size, and randomization

For the generation of *Tg779* mice, *Mhrt779* was cloned into pTRE2 backbone (Clonetech, CA). DNA fragment containing the Tre promoter, and *Mhrt779* was injected into the pronucleus of fertilized oocytes (B6C3H/F1). Embryos were implanted into a pseudopregnant CD-1 mouse. *Tre-Mhrt779* transgene was identified by PCR genotyping using primers (CGCCTGGAGACGCCATCCAC; TGTCTTCAAAGCTGACTCCCT). *Tre-Mhrt779* mice with ~3 copies of the transgene were backcrossed with *Tnnt2-rtTA* mice as described previously[3,30] to generate *Tnnt2-rtTA; Tre-Mhrt779* (*Tg779*) mice. The number of animals used (N) was denoted in each test in the figures, including technical replicates when applicable. We routinely used mouse littermates to control and perform our experiments. Each subgroup of experiments had N = 3 to 14 biological replicates, many of which had technical replicates of three. The assignment to each experimental subgroup was based on the genotypes. Littermate mice with the same genotypes regardless of gender were randomly selected from the cage and assigned to different control and experimental subgroups. Major procedures were blinded. The use of mice for studies was in compliance with the regulations of Indiana University, Stanford University, and National Institute of Health.

RACE and cloning of full length of *Mhrt* transcripts

The 3′ and 5′ RACE were performed using the FirstChoice RLM-RACE Kit (Ambion) following the manufacture's instruction. RNA was extracted from adult heart ventricles. Primers used for 3′ and 5′ RACE were designed based on the known sequence information: TCATTGGCACGGACAGCATC (First-round *Mhrt* 3′-prime specific) and GAGCATTTGGGGATGGTATAC (Second-round *Mhrt* 3′-prime specific); CAACACTTTTCATTTTCCTCTTT (First-round *Mhrt* 5′-prime specific) and TCTGCTTCATTGCCTCTGTTT (Second-round *Mhrt* 5′-prime specific). Once we reached the 5′- and 3′-cDNA ends, we used primers F1 (Fig. 1a, AAGAGCCCTACAGTCTGATGAACA) and R1 Fig. 1a, CCTTCACACAAACATTTTATTT) to amply the full-length *Mhrt* transcripts and cloned into pDrive TA cloning vector (Qiagen) and send for sequencing. *Mhrt*s were also further cloned into shuttle vector pAdd2[31,32] for expression in cells.

Northern blot and *in situ* Hybridization

We obtained 5 μg of total RNA using Quick-RNA Mini Kit (Zymo Research). RNA blot was performed using NorthernMax Kit (Ambion) following the manufacturer's protocol. Single stranded RNA probe was generated by *in vitro* transcription with MaxIscript SP6/T7 kit (Ambion) with ATP [α-^{32}P] (PerkinElmer) using full-length *Mhrt779*, *Myh6* and *Myh7* as the template and followed by digestion with DNase I (Ambion). Hybridization was performed at 65°C. The blot was washed and imaged by Phosphor storage scanning by Typhoon 8600 Imager (GE Healthcare). *In situ* hybridization experiments were performed as previously described[3,33].

RNA fractionation

To isolate cytosolic and nuclear RNAs from adult heart tissues, we used PARIS kit (Ambion) and followed the manufacturer's instruction. 10 mg of tissues were homogenized in Cell Fractionation Buffer thoroughly before centrifuge for 5min at 500g. Supernatant was collected as cytosolic fraction, while nuclear pellet was washed and lysed by Cell Disruption Buffer. Such samples were further mixed with 2X Lysis/Binding Solution before extracting RNA using the manufacturer's protocol.

Codon substitution frequency predication

To measure the coding potential of *Mhrt*, we used the previously described codon substitution frequencies (CSF) method[4,5] to evaluate the evolutionary characteristics in their alignments with orthologous regions in 6 other sequenced mammalian genomes (Rat, Human, Hamster, Rhesus Monkey, Cat and Dog). CSF generates a likelihood score for a given sequence considering all codon substitutions observed within its alignment across multiple species, which was based on the relative frequency of similar substitutions occurred in known coding and noncoding regions. CSF compares two empirical codon models; one generated from alignments of known coding regions and the other according to noncoding regions, producing a likelihood ratio. The ratio reflects whether the protein-coding model better explains the alignment.

Ribosome profiling and RNA deep sequencing

For ribosome profiling[6], over-expression of predominant specie of *Mhrt* (*Mhrt779*) along with *HOTAIR* were achieved through co-transfecting pAdd2-779 and pAdd2-HOTAIR into SW13 cells. The cells were then lysed to extract ribosome-associated RNA fragments using ARTseq™ Ribosome Profiling Kit (Epicenter, Illumina). The RNA fragments were further converted into a DNA library through end repair, adaptor ligation, reverses transcription circularization, and PCR amplification. A conventional RNA-seq library was also prepared with total RNA extracted from those cells with miRNeasy Mini Kit (Qiagen #217004). The libraries were further processed according to MiSeq Sample Prep sheet, and MiSeq 50 cycle kit was used for sequencing. 1.25 picomoles PCR products were used for sequencing. 600K~700K reads were properly paired and used for further analysis. The resulting reads were aligned to the human hg19 or mouse mm10 genome using Bowtie2 v2.0.0.6[34]. Mapped reads were visualized on the UCSC browser as bigwig files generated using samtools v0.1.18[35], bedtools v2.16.1[36], bedClip and bedGraphToBigWig. For quantification of FPKM values (fragments per kilobase of exon per million fragments mapped), cuffdiff as part of the tophat suite V2.0.8b[37] was run on a merged bam file containing the human and the *Mhrt* reads using a custom gtf file comprising of the human hg19 iGenome and the *Mhrt* transcripts. To generate scatter plot of the genes, cuffdiff files were used for visualization with cummerbund v2.3.1[37]. The data were uploaded to GEO (Gene Expression Omnibus) with accession number: GSE49716.

In vitro translation and biotin labeling

TNT Quick Coupled Transcription/Translation System (Promega) was used for *in vitro* translation. Briefly, 1 ug plasmids of control (*Luciferase*) and various *Mhrt* species inserted into pDrive vector were added to 40 ul rabbit reticulocyte lysates containing S^{35}-methionine. After 1hr of incubation, the reactions were analyzed on 10–20% Tris-Tricine gel. The gel was dried and visualized by the Typhoon 8600 Imager (GE Healthcare). Biotin-NTP was added to *in vitro* translation reaction. Total RNAs were extracted and the biotin-labeled RNAs were detected subsequently by IRDye 680 Streptavidin (Li-COR, 926-68079) using Odyssey Infrared Imaging System.

Transaortic constriction (TAC)

The TAC surgery was performed as described[3] on adult mice of 8–10 weeks of age and between 20 and 25 grams of weight. Mice were fed with doxycycline food pellets (6 mg doxycycline/kg of food, Bioserv, Frenchtown, NJ) 7–14 days prior to the TAC operation. Mice were anesthetized with isoflurane (2–3%, inhalation) in an induction chamber and then intubated with a 20-gauge intravenous catheter and ventilated with a mouse ventilator (Minivent, Harvard Apparatus, Inc). Anesthesia was maintained with inhaled isoflurane (1–2%). A longitudinal 5-mm incision of the skin was made with scissors at midline of sternum. The chest cavity was opened by a small incision at the level of the second intercostal space 2–3 mm from the left sternal border. While opening the chest wall, the chest retractor was gently inserted to spread the wound 4–5 mm in width. The transverse portion of the aorta was bluntly dissected with curved forceps. Then, 6–0 silk was brought underneath the transverse aorta between the left common carotid artery and the brachiocephalic trunk. One

27-gauge needle was placed directly above and parallel to the aorta. The loop was then tied around the aorta and needle, and secured with a second knot. The needle was immediately removed to create a lumen with a fixed stenotic diameter. The chest cavity was closed by 6–0 silk suture. Sham-operated mice underwent similar surgical procedures, including isolation of the aorta, looping of aorta, but without tying of the suture. The pressure load caused by TAC was verified by the pressure gradient across the aortic constriction measured by echocardiography. Only mice with a pressure gradient >30 mmHg were analyzed for cardiac hypertrophy, echocardiography and other purposes.

Echocardiography

The echocardiographer was blinded to the genotypes and surgical procedure. Transthoracic ultrasonography with a GE Vivid 7 ultrasound platform (GE Health Care, Milwaukee, WI) and a 13 MHz transducer was used to measure aortic pressure gradient and left ventricular function. Echocardiography was performed on control and *Tnnt2-rtTA*;*Tre-Mhrt779* (*Tg779*) mice designated time points after the TAC procedure. To minimize the confounding influence of different heart rates on aortic pressure gradient and left ventricular function, the flow of isoflurane (inhalational) was adjusted to anesthetize the mice while maintaining their heart rates at 450–550 beats per minute. The peak aortic pressure gradient was measured by continuous wave Doppler across the aortic constriction. The left ventricular function was assessed by the M-mode scanning of the left ventricular chamber, standardized by two-dimensional, short-axis views of the left ventricle at the mid papillary muscle level. Left ventricular (LV) chamber size and wall thickness were measured in at least three beats from each projection and averaged. LV internal dimensions at diastole and systole (LVIDd and LVIDs, respectively) were measured. The fractional shortening (FS) of the left ventricle was defined as 100% × (1 - LVIDs/LVIDd), representing the relative change of left ventricular diameters during the cardiac cycle. The mean FS of the left ventricle was determined by the average of FS measurement of the left ventricular contraction over 5 beats. P-values were calculated by the Student-t test. Error bars indicate standard error of mean.

Histology, trichrome staining, and morphometric analysis of cardiomyocytes

Histology and trichrome staining were performed as described[38,39]. Trichrome Stain (Masson) kit (Sigma) was used and manufacture's protocol was followed. For morphometric analysis of cardiomyocytes, paraffin sections of the heart were immunostained with a fluoresecin isothiocyanate-conjugated Wheat Germ Agglutinin (WGA) antibody (F49, Biomeda, Foster City, CA) that highlighted the cell membrane of cardiomyocytes. Cellular areas outlined by WGA were determined by the number of pixels enclosed using Image J software (NCBI). Approximately 250 cardiomyocytes of the papillary muscle at the mid left ventricular cavity were measured to determine the size distribution. P-values were calculated by the Student-t test. Error bars indicate standard error of mean.

Reverse transcription–quantitative PCR analysis (RT–qPCR) and strand specific reverse transcription PCR analysis

RT–qPCR analyses were performed as described[3,38]. The following primer sequences (listed below) were used. RT-qPCR reactions were performed using SYBR green master mix

(BioRad) with an Eppendorf realplex, and the primer sets were tested to be quantitative. Threshold cycles and melting curve measurements were performed with software. P-values were calculated by the Student-t test. Error bars indicate standard error of mean. To conduct strand specific RT PCR analysis, human total RNA and Superscript III First-Strand Synthesis System (Invitrogen) was used. Primers R1 (Fig. 4k, CTACAGAATGAGATCGAGGACT) and R2 (Fig. 4k, GGGGCTGAAGAGTGAGCCTT) were designed based on known sequence and used for individual RT respectively. To detect *MHRT*, primers F1 (Fig. 4k, CTGGAGCTGGGACAGGTCAGCA) and R1 were used. Those primers could also amplify endogenous *MYH7* and thus serve as controls. Primers F2 (Fig. 4k, TGGGGAACACGGCGTTCTTGA) and R2 were used to specifically amplify *MHRT* and used in RT-qPCR analysis.

PCR primers for RT-qPCR *of mRNA:*

Mouse *TfIIb*-F (CTCTGTGGCGGCAGCAGCTATTT),

Mouse *TfIIb*-R (CGAGGGTAGATCAGTCTGTAGGA),

Mouse *Hprt1*-F (GCTGGTGAAAAGGACCTCT),

Mouse *Hprt1*-R (CACAGGACTAGAACACCTGC),

Mouse *Anf*-F (GACTAGGCTGCAACAGCTTCCG),

Mouse *Anf*-R (GCCACAGTGGCAATGTGACCAA),

Mouse *Serca2a*-F (CATTTGCATTGCAGTCTGGAT),

Mouse *Serca2a*-R (CTTTGCCATCCTACGAGTTCC),

Mouse *Tnnt2*-F (TACAGACTCTGATCGAGGCTCACTTC),

Mouse *Tnnt2*-R (TCATTGCGAATACGCTGCTGCTC),

Mouse *Mhrt*-F (common) (GAGCATTTGGGGATGGTATAC),

Mouse *Mhrt*-R (common) (TCTGCTTCATTGCCTCTGTTT),

Mouse *Mhrt779*-F (TCTGGCCACAGCCCGCAGCTTC),

Mouse *Mhrt779*-R (AGTCATGTATACCATCCCCAA),

Mouse *Neat1*-F (TCTCCTGGAGCCACATCTCT)

Mouse *Neat1*-R (GCTTTTCCTTAGGCCCAAAC)

Mouse 28S-rRNA-F (GGTAGCCAAATGCCTCGTCAT)

Mouse 28S-rRNA-R (CCCTTGGCTGTGGTTTCG)

Human *TFIIb*-F (ACCACCCCAATGGATGCAGACAG),

Human *TFIIb*-F (ACGGGCTAAGCGTCTGGCAC),

Human *MHRT*-F (F2, TGGGGAACACGGCGTTCTTGA),

Human *MHRT*-R (R2, GGGGCTGAAGAGTGAGCCTT).

Human *HOTAIR*-F (GGTAGAAAAAGCAACCACGAAGC)

Human *HOTAIR*-R (ACATAAACCTCTGTCTGTGAGTGCC)

Human *GAPDH*-F (CCGGGAAACTGTGGCGTGATGG)

Human *GAPDH*-R (AGGTGGAGGAGTGGGTGTCGCTGTT)

Chromatin immunoprecipitation–quantitative PCR (ChIP–qPCR)

ChIP assay was performed as described[3] with modifications. Briefly, chromatin from hearts or SW13 cells was sonicated to generate average fragment sizes of 200–600 bp, and immunoprecipitated using anti-BRG1 J1 antibody[3,40], anti-Brg1 H-10 antibody (Santa Cruz Biotechnology, against 115–149 amino acids of N-terminus Brg1), anti-RNA polymerase II (Pol II) antibody (ab24759, Abcam), anti-H3K4me3 antibody (07–473, Millipore), anti-H3K36me3 antibody (17–10032, Millipore) or normal control IgG. Isolation and purification of immunoprecipitated and input DNA were done according to the manufacturer's protocol (Magna ChIP Protein G Magnetic Beads, Millipore), and qPCR analysis of immunoprecipitated DNA were performed. ChIP–qPCR signal of individual ChIP reaction was standardized to its own input qPCR signal or IgG ChIP signal. PCR primers (listed below) were designed to amplify the promoter regions of mouse *Myh6* (−426, −320), mouse *Myh7* (−102, +58), mouse *Shh* (−7142, −6911), mouse *Vegfa* (+1, +150) human *GAPDH* (−45, +121). The DNA positions are denoted relative to the transcriptional start site (+1).

PCR primers for ChIP-qPCR:

Mouse ChIP-*Myh6* promoter-F (GCAGATAGCCAGGGTTGAAA),

Mouse ChIP-*Myh6* promoter-R (TGGGTAAGGGTCACCTTCTC),

Mouse ChIP-*Myh7* promoter-F (GTGACAACAGCCCTTTCTAAAT),

Mouse ChIP-*Myh7* promoter-R (CTCCAGCTCCCACTCCTACC),

Mouse ChIP-*Shh* promoter-F (GAGAACATTACAGGGTAGGAA),

Mouse ChIP-*Shh* promoter-R (GAAGCAGTGAGGTTGGTGG),

Mouse ChIP-*Vegfa* promoter-F (CAAATCCCAGAGCACAGACTC),

Mouse ChIP-*Vegfa* promoter-R (AGCGCAGAGGCTTGGGGCAGC),

Human ChIP-*GAPDH* promoter-F (TACTAGCGGTTTTACGGGCG),

Human ChIP-*GAPDH* promoter-R (TCGAACAGGAGGAGCAGAGAGCGA).

RNA Immunoprecipitation

RNA Immunoprecipitation (RNA-IP, RIP) was conducted as described[4] with some modifications. Briefly, P1 hearts, sham/TAC'ed hearts, or SW13 cells were cross-linked and lysed with Lysis Buffer (10 mM HEPES pH 7.5, 85 mM KCl, 0.5% NP-40, 1 mM DTT, 1 × protease inhibitor) for tissue and Lysis Buffer (10 mM Tris-HCl pH 8.1, 10 mM NaCl, 1.5 mM $MgCl_2$, 0.5% NP-40, 1 mM DTT, 1X protease inhibitor) for cell. Nuclei were isolated and sonicated using Bioruptor (Diagenode) (30 s on, 30 s off, power setting H, 5 minute for twice) in Nuclear Lysis buffer (50 mM Tris-HCl pH 8.1, 150 mM NaCl, 0.1% NP-40, 1 mM DTT, protease inhibitor, Ribonuclease inhibitor). The nuclear extract was collected and incubated with primary antibodies at 4°C for overnight together with Manga ChIP Protein G Magnetic Beads (Millipore). The beads were washed by Wash Buffer I (20 mM Tris-Hcl pH 8.1, 150 mM NaCl, 1% Triton X-100 and 0.1% SDS) for three times, and Wash Buffer II (20 mM Tris-Hcl pH 8.1, 500 mM NaCl, 1% Triton X-100 and 0.1% SDS) for three times. Beads were then resuspended in 150 μl 150 mM RIPA (50 mM Tris pH 7.5, 150 mM NaCl, 1 mM EDTA, 0.1% SDS, 1% NP-40, 0.5% sodium deoxycholate) with 5 μl Proteinase K and incubated for 1 h at 65°C. We added 1 ml of TRIzol to the sample, and RNA was extracted using the Quick-RNA Mini Kit with the on-column DNAse I digest (ZymoResearch). RT and qPCR were then conducted with the purified RNA. The antibodies used for the immunoprecipitation are anti-BRG1 J1 antibody[3,40], Ezh2[41] (Active Motif), Suz12[41,42] (Bethyl Laboratories) and normal IgG control.

Reporter assay and truncation of *Mhrt* promoter

For *Mhrt* promoter reporter assay, plasmid was constructed by inserting ~2.5Kbp mouse *Mhrt* promoter into the episomal pREP4-Luc plasmid[3,19,38,43] through cloning PCR amplified region of the promoter by using primers ACCGGCCTGAACCCCACTTCC and ATGTCGAGACAGGGAACAGAA. Mouse *Myh6* (−426 to +170, based on new genome annotation) and *Myh7* (−3561 to +222) reporter constructs were described previously[3]. These vectors were transfected into rat neonatal cardiomyocytes or SW13 cells using lipofectamine 2000 (Invitrogen) along with plasmids expressing mouse Brg1 (Actin-mBrg1-IRES-EGFP) or a matching empty vector plasmid (Gifts from Dr. G. Crabtree) as well as an episomal renilla-luciferase plasmid (pREP7-RL) to normalize transfection efficiency. The transfected cells were cultured for 48hrs and harvested for luciferase assay using the dual luciferase assay kit (Promega). For naked DNA reporter, mouse *Myh6* promoter (−426 to +170) was inserted in pGL3 vector (Promega), and renilla-luciferase plasmid phRL-SV40 (Gifts from Dr. J. Chen) was used as a normalizer. Dual luciferase assay was performed according to the manufacture's instruction 48hrs after transfection. For deletional analysis of *Mhrt* promoter, various regions of the promoter were deleted from the full-length pREP4-*Mhrt*. The constructs were further analysed by transfecting into SW13 cells.

RNA-EMSA and *Kd* calculation

Biotin-labeled RNA probe was generated by *in vitro* transcription with MAXIscript SP6/T7 kit (Ambion) with biotin labeling NTP mixture (Roche) using linearized pDrive-*Mhrt779*

construct as the template and followed by digestion with DNase I (Ambion). The EMSA was performed by using the LightShift Chemiluminescent RNA EMSA Kit (Thermo Scientific). The labeled probe was incubated with appropriate amount of recombinant proteins in 10 μl in the 1 × binding buffer (10 mM HEPES-KOH, pH 7.3, 10 mM NaCl, 1 mM $MgCl_2$, 1 mM DTT) with 5 μg tRNA carrier at room temperature for 30 min. The reactions were then loaded onto 1% 0.5 × TBE agarose gel and transferred to BrightStar-Plus positive charged membrane. The biotin-labeled probes were detected and quantified subsequently by IRDye 680 Streptavidin (Li-COR, 926–32231) using Odyssey Infrared Imaging System. The shifted signals were quantified and plotted against amount of the MBP, MBP-D1, MBP-D2 and MBP-D1D2 proteins using previously described method[26] with GraphPad Prism (GraphPad). The software facilitates the fitting of non-linear regression model and calculation of *Kd*s (Dissociate Constant) based on the fitting curve. The errors and r-square (r^2) were also generated from the fitting curve.

Protein expression and purification of Brg1 helicase domains

To generate MBP fusion proteins of mouse Brg1 helicase domains, the DExx-box domain (D1) (Amino acids 774–913 of Brg1), Helicase-C domain (D2) together with carboxyl-terminal extension (CTE) (Amino acids 1086–1310 of Brg1), as well as the entire helicase region (D1D2) (774–1310) were amplified by PCR and cloned into pMAL vector. MBP fusion proteins were induced by IPTG and purified by Amylose resin (E8021S, NEB).

Nucleosome assembly and amylose pull-down

Nucleosome assembly was performed by using EpiMark Nucleosome Assembly Kit (E5350S, NEB) following the manufacture's instruction[28]. In brief, recombinant human core histone octamer, which consist of the 2:1 mix of histone H2A/H2B dimer and histone H3.1/H4 tetramer, were mixed with purified 5SrDNA (208bp, N1202S, NEB), *Neo* (512bp, amplified from pST18-*Neo*, 1175025, Roche), *Myh6* core promoter (596bp, −426 to +170) and *Mhrt* core promoter (a3a4, 596bp, −2290 to −1775) DNA at 2 M NaCl. PCR primers to amplify *Neo* are CGATGCGCTGCGAATCGGGA and CACTGAAGCGGGAAGGGACT. The salt concentration was gradually lowered by dilution to allow the formation of nucleosomes. The EMSA assay was used to assess the efficiency of nucleosome assembly. For amylose pull-down assay, the amylose resin (E8021S, NEB) was washed thoroughly and equilibrated with binding buffer (10 mM Tris-HCl, pH=7.5, 150 mM NaCl) before incubation with purified MBP, MBP-D1D2 proteins for 2hr. Nucleosome mixture or naked DNA mixture of 5S rDNA, *Neo* and *Myh6* promoter DNA were added for incubation at 4°C for overnight. The resin was then washed excessively by washing buffer (20 mM Tris-HCl, pH=8.1, 150 mM NaCl, 2 mM EDTA, 1% Triton X-100, 0.1% SDS) before decrosslinking and extraction of the DNA with Phenol: Chloroform: Isoamyl Alcohol. For competition assay, *in vitro* transcribed *Mhrt779* was incubated with MBP-D1D2 in binding buffer (10 mM HEPES-KOH, pH 7.3, 10 mM NaCl, 1 mM $MgCl_2$, 1 mM DTT) with Ribonuclease inhibitor at room temperature for 30 minutes before adding nucleosomal DNA. The subsequent incubation, wash and DNA purification were performed as regular amylose pull-down assays. qPCR signal of individual pull-down reaction was standardized to its own input RT-qPCR signal. qPCR primers were designed to amplify the 5SrDNA (CAAGCAAGAGCCTACGACCA; ATTCGTTGGAATTCCTCGGG), *Neo*

(TAAAGCACGAGGAAGCGGTC; TCGACCACCAAGCGAAACAT), *Myh6* promoter (GCAGATAGCCAGGGTTGAAA; TGGGTAAGGGTCACCTTCTC) and *Mhrt* promoter (ATGCCAAATGGTTGCTCTTT; GAGCTTGAGAACCAGGCAGT).

Cloning of Brg1 truncation constructs

For cloning of the truncated Brg1 with deletion of amino acids 774–913 (ΔD1) or 1086–1246 (ΔD2), the primers with NheI restriction digestion site, which complement with the downstream and upstream of the truncated region (Δ D1: CCCGGGGCTAGCCTGCAGAACAAGCTACCGGAGCT and CCCGGGGCTAGCCAGGTTGTTGTTGTACAGGGACA; Δ D2: CCCGGGGCTAGCATCAAGAAGTTCAAATTTCCC and CCCGGGGCTAGCCTGCAGGCCATCCTGGAGCACGAGCAG) were used to amplify from pActin-Brg1-IRES-EGFP by KOD Xtreme Hot Start DNA Polymerase (Novagen). After digestion with NheI, the linearized fragment was subject to ligation and transformation. The truncation constructs were sequenced to confirm the fidelity of the cloning. Western Blot was further performed to assess the expression of the constructs. Monoclonal H-10 antibody (Santa Cruz Biotech, sc-374197), which were raised against Brg1 N-terminal amino acids, were used in the experiments involving the truncated Brg1.

Protein sequence analysis

Brg1 core helicase domain (774–1202) was applied for secondary structure prediction using the Fold & Function Assignment System (FFAS) server (http://ffas.burnham.org/ffas-cgi/cgi/ffas.pl). The output revealed that Brg1 core helicase domain are structural homologs of SF2 helicases: Vasa[44] (Fruit fly, PDB# 2DB3), Rad54[27,45] (Zebrafish PDB# 1Z3I, *Sulfolobus solfataricus* PDB# 1Z63) and Chd1[46] (Yeast, PDB# 3MWY). Those proteins together with Brg1 were further employed for multiple sequence alignment with T-Coffee, which is a program allowing combination of the results obtained with several alignment methods (http://www.ebi.ac.uk/Tools/msa/tcoffee/).

RNA secondary structural prediction

To predict the secondary structure for mouse *Mhrt* and human *MHRT*, the single stranded sequence of *Mhrt779* and human *MHRT* were analyzed on the Vienna RNAfold web server (http://rna.tbi.univie.ac.at/cgi-bin/RNAfold.cgi) with calculation of minimum free energy[29,47-49].

Human heart tissue analysis

The human tissues were processed for RT-qPCR and strand-specific RT-PCR. The use of human tissues is in compliance with the regulation of Sanford/Burnham Medical Research Institute, Intermountain Medical Center, Stanford University, and Indiana University.

Primary cardiomyocyte culture

For functional studies in cardiomyocytes, neonatal rat ventricular cardiomyocytes were cultured as previously described[50,51]. Briefly, P0 or P1 Sprague-Dawley rats were used. The ventricles were excised and trypsinized for 15 minutes for 4–5 times. Cells were then

collected and resuspended in DMEM supplements with 10% FBS. The cells were plated for 1 h to allow the attachment of non-cardiomyocytes cells. The remaining cardiomyocytes were plated at a density of 2×10^5/ml. The cells were transfected with Lipofectamine 2000 (Invitrogen) after 48 hr.

Supplementary Material

Refer to Web version on PubMed Central for supplementary material.

Acknowledgements

We thank C-H Chen for assisting with echocardiography; L. Chen, A. Kuo and G. Crabtree for transgene injection and northern blot; M. Ecarkt and E. Zuo for ribosome analysis. C-P.C. was supported by American Heart Association (AHA, Established Investigator Award 12EIA8960018). National Institutes of Health (NIH, HL118087, HL121197), March of Dimes Foundation ((#6-FY11-260), California Institute of Regenerative Medicine (CIRM, RN2-00909), Oak Foundation, Stanford Heart Center Research Program, Indiana University (IU) School of Medicine-IU Health Strategic Research Initiative, and IU Physician-Scientist Initiative, endowed by Lilly Endowment, Inc. W.L. and Y.X. were supported by Oak Foundation; Y.X. by AHA and Lucile Packard Children's Foundation; C.S. by NIH fellowship; H-S.V.C by CIRM (RB2-01512, RB4-06276) and NIH (HL105194); B.Z. by NIH (HL116997, HL111770).

References and Notes

1. Katayama S, et al. Antisense transcription in the mammalian transcriptome. Science. 2005; 309:1564–1566. [PubMed: 16141073]
2. Haddad F, Bodell PW, Qin AX, Giger JM, Baldwin KM. Role of antisense RNA in coordinating cardiac myosin heavy chain gene switching. J Biol Chem. 2003; 278:37132–37138. [PubMed: 12851393]
3. Hang CT, et al. Chromatin regulation by Brg1 underlies heart muscle development and disease. Nature. 2010; 466:62–67. [PubMed: 20596014]
4. Hung T, et al. Extensive and coordinated transcription of noncoding RNAs within cell-cycle promoters. Nat Genet. 2011; 43:621–629. [PubMed: 21642992]
5. Lin MF, Jungreis I, Kellis M. PhyloCSF: a comparative genomics method to distinguish protein coding and non-coding regions. Bioinformatics. 2011; 27:i275–282. [PubMed: 21685081]
6. Ingolia NT, Brar GA, Rouskin S, McGeachy AM, Weissman JS. The ribosome profiling strategy for monitoring translation in vivo by deep sequencing of ribosome-protected mRNA fragments. Nat Protoc. 2012; 7:1534–1550. [PubMed: 22836135]
7. van Rooij E, et al. Control of stress-dependent cardiac growth and gene expression by a microRNA. Science. 2007; 316:575–579. [PubMed: 17379774]
8. Miyata S, Minobe W, Bristow MR, Leinwand LA. Myosin heavy chain isoform expression in the failing and nonfailing human heart. Circ Res. 2000; 86:386–390. [PubMed: 10700442]
9. Lompre AM, et al. Myosin isoenzyme redistribution in chronic heart overload. Nature. 1979; 282:105–107. [PubMed: 91973]
10. Schultz Jel J, et al. TGF-beta1 mediates the hypertrophic cardiomyocyte growth induced by angiotensin II. J Clin Invest. 2002; 109:787–796. [PubMed: 11901187]
11. Molkentin JD, Dorn GW 2nd. Cytoplasmic signaling pathways that regulate cardiac hypertrophy. Annual review of physiology. 2001; 63:391–426.
12. Lopez B, et al. Osteopontin-mediated myocardial fibrosis in heart failure: a role for lysyl oxidase? Cardiovascular research. 2013; 99:111–120. [PubMed: 23619422]
13. Frey N, Olson EN. Cardiac hypertrophy: the good, the bad, and the ugly. Annual review of physiology. 2003; 65:45–79.
14. Guttman M, et al. Chromatin signature reveals over a thousand highly conserved large non-coding RNAs in mammals. Nature. 2009; 458:223–227. [PubMed: 19182780]

15. Rando OJ, Chang HY. Genome-wide views of chromatin structure. Annu Rev Biochem. 2009; 78:245–271. [PubMed: 19317649]
16. Hahn MA, Wu X, Li AX, Hahn T, Pfeifer GP. Relationship between gene body DNA methylation and intragenic H3K9me3 and H3K36me3 chromatin marks. PLoS One. 2011; 6:e18844. [PubMed: 21526191]
17. Mikkelsen TS, et al. Genome-wide maps of chromatin state in pluripotent and lineage-committed cells. Nature. 2007; 448:553–560. [PubMed: 17603471]
18. Musselman CA, et al. Molecular basis for H3K36me3 recognition by the Tudor domain of PHF1. Nat Struct Mol Biol. 2012; 19:1266–1272. [PubMed: 23142980]
19. Liu R, et al. Regulation of CSF1 promoter by the SWI/SNF-like BAF complex. Cell. 2001; 106:309–318. [PubMed: 11509180]
20. Muchardt C, Yaniv M. A human homologue of Saccharomyces cerevisiae SNF2/SWI2 and Drosophila brm genes potentiates transcriptional activation by the glucocorticoid receptor. Embo J. 1993; 12:4279–4290. [PubMed: 8223438]
21. Szabo G, et al. Poly(ADP-Ribose) polymerase inhibition reduces reperfusion injury after heart transplantation. Circ Res. 2002; 90:100–106. [PubMed: 11786525]
22. Hesselberth JR, et al. Global mapping of protein-DNA interactions in vivo by digital genomic footprinting. Nat Methods. 2009; 6:283–289. [PubMed: 19305407]
23. Gupta MP. Factors controlling cardiac myosin-isoform shift during hypertrophy and heart failure. J Mol Cell Cardiol. 2007; 43:388–403. [PubMed: 17720186]
24. Clapier CR, Cairns BR. The biology of chromatin remodeling complexes. Annu Rev Biochem. 2009; 78:273–304. [PubMed: 19355820]
25. Jankowsky E, Fairman ME. RNA helicases--one fold for many functions. Curr Opin Struct Biol. 2007; 17:316–324. [PubMed: 17574830]
26. Mallam AL, Del Campo M, Gilman B, Sidote DJ, Lambowitz AM. Structural basis for RNA-duplex recognition and unwinding by the DEAD-box helicase Mss116p. Nature. 2012; 490:121–125. [PubMed: 22940866]
27. Durr H, Korner C, Muller M, Hickmann V, Hopfner KP. X-ray structures of the Sulfolobus solfataricus SWI2/SNF2 ATPase core and its complex with DNA. Cell. 2005; 121:363–373. [PubMed: 15882619]
28. Feng Y, et al. Histone H4 acetylation differentially modulates arginine methylation by an in Cis mechanism. J Biol Chem. 2011; 286:20323–20334. [PubMed: 21502321]
29. Zuker M. On finding all suboptimal foldings of an RNA molecule. Science. 1989; 244:48–52. [PubMed: 2468181]
30. Wu B, et al. Inducible cardiomyocyte-specific gene disruption directed by the rat Tnnt2 promoter in the mouse. Genesis. 2010; 48:63–72. [PubMed: 20014345]
31. Wei K, Kuhnert F, Kuo CJ. Recombinant adenovirus as a methodology for exploration of physiologic functions of growth factor pathways. J Mol Med (Berl). 2008; 86:161–169. [PubMed: 17891365]
32. Kuhnert F, et al. Essential regulation of CNS angiogenesis by the orphan G protein-coupled receptor GPR124. Science. 2010; 330:985–989. [PubMed: 21071672]
33. Xiong Y, et al. Brg1 governs a positive feedback circuit in the hair follicle for tissue regeneration and repair. Dev Cell. 2013; 25:169–181. [PubMed: 23602386]
34. Langmead B, Salzberg SL. Fast gapped-read alignment with Bowtie 2. Nat Methods. 2012; 9:357–359. [PubMed: 22388286]
35. Li H, et al. The Sequence Alignment/Map format and SAMtools. Bioinformatics. 2009; 25:2078–2079. [PubMed: 19505943]
36. Quinlan AR, Hall IM. BEDTools: a flexible suite of utilities for comparing genomic features. Bioinformatics. 2010; 26:841–842. [PubMed: 20110278]
37. Trapnell C, et al. Differential gene and transcript expression analysis of RNA-seq experiments with TopHat and Cufflinks. Nat Protoc. 2012; 7:562–578. [PubMed: 22383036]
38. Stankunas K, et al. Endocardial Brg1 represses ADAMTS1 to maintain the microenvironment for myocardial morphogenesis. Dev Cell. 2008; 14:298–311. [PubMed: 18267097]

39. Chang CP, et al. A field of myocardial-endocardial NFAT signaling underlies heart valve morphogenesis. Cell. 2004; 118:649–663. [PubMed: 15339668]
40. Khavari PA, Peterson CL, Tamkun JW, Mendel DB, Crabtree GR. BRG1 contains a conserved domain of the SWI2/SNF2 family necessary for normal mitotic growth and transcription. Nature. 1993; 366:170–174. [PubMed: 8232556]
41. Grote P, et al. The tissue-specific lncRNA Fendrr is an essential regulator of heart and body wall development in the mouse. Dev Cell. 2013; 24:206–214. [PubMed: 23369715]
42. Klattenhoff CA, et al. Braveheart, a long noncoding RNA required for cardiovascular lineage commitment. Cell. 2013; 152:570–583. [PubMed: 23352431]
43. van der Vlag J, den Blaauwen JL, Sewalt RG, van Driel R, Otte AP. Transcriptional repression mediated by polycomb group proteins and other chromatin-associated repressors is selectively blocked by insulators. J Biol Chem. 2000; 275:697–704. [PubMed: 10617669]
44. Sengoku T, Nureki O, Nakamura A, Kobayashi S, Yokoyama S. Structural basis for RNA unwinding by the DEAD-box protein Drosophila Vasa. Cell. 2006; 125:287–300. [PubMed: 16630817]
45. Thoma NH, et al. Structure of the SWI2/SNF2 chromatin-remodeling domain of eukaryotic Rad54. Nat Struct Mol Biol. 2005; 12:350–356. [PubMed: 15806108]
46. Hauk G, McKnight JN, Nodelman IM, Bowman GD. The chromodomains of the Chd1 chromatin remodeler regulate DNA access to the ATPase motor. Mol Cell. 2010; 39:711–723. [PubMed: 20832723]
47. Zuker M, Stiegler P. Optimal computer folding of large RNA sequences using thermodynamics and auxiliary information. Nucleic Acids Res. 1981; 9:133–148. [PubMed: 6163133]
48. Gruber AR, Lorenz R, Bernhart SH, Neubock R, Hofacker IL. The Vienna RNA websuite. Nucleic Acids Res. 2008; 36:W70–74. [PubMed: 18424795]
49. Wan Y, Kertesz M, Spitale RC, Segal E, Chang HY. Understanding the transcriptome through RNA structure. Nature reviews. Genetics. 2011; 12:641–655.
50. Fu XM, Yao YJ, Yang Z, Xiang L, Gao J. Alteration and its significance to expression of aquaporin-4 in cultured neonatal rat astrocytes in the model of hypoxic damage. Sichuan Da Xue Xue Bao Yi Xue Ban. 2005; 36:641–644. [PubMed: 16235526]
51. Yang J, et al. C-reactive protein augments hypoxia-induced apoptosis through mitochondrion-dependent pathway in cardiac myocytes. Molecular and cellular biochemistry. 2008; 310:215–226. [PubMed: 18165866]

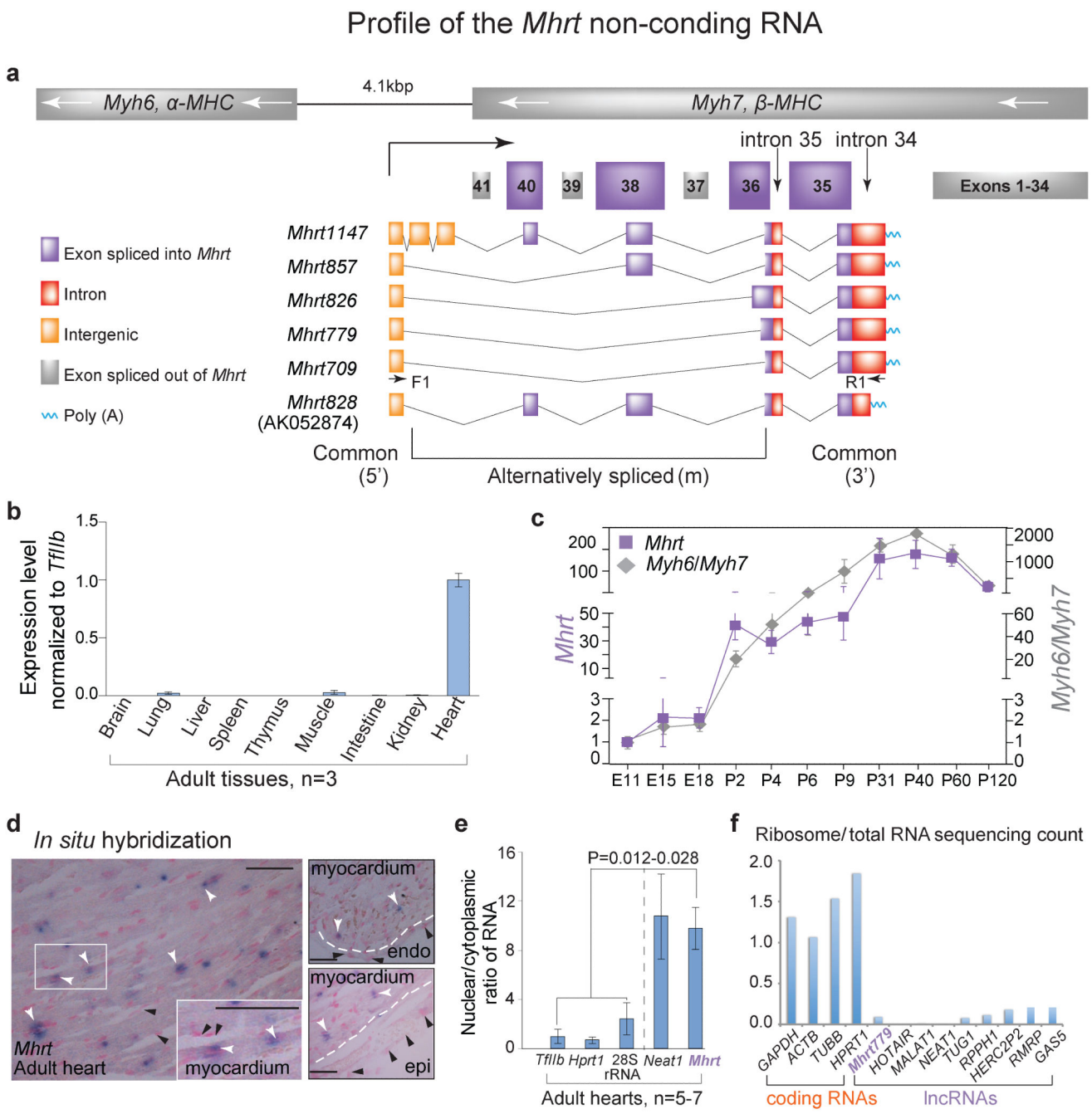

Figure 1. Profile of the non-coding RNA *Mhrt*

a, Schematic illustration of *Mhrt*s originating from the intergenic region between *Myh6* and *Myh7* and transcribed into *Myh7*. *Myh7* exons and introns are indicated. F1 and R1, targeting 5' and 3′ *Mhrt* common sequences, are the primers used for subsequent PCR.

b, RT-qPCR of *Mhrts* using primers targeting common regions of *Mhrts* in tissues from 2-month-old mice. P-value: Student's t-test. Error bar: standard error of the mean (SEM).

c, RT-qPCR of *Mhrt*, *Myh6* and *Myh7* in mouse hearts at different ages. *Mhrt* and *Myh6*/*Myh7* ratio of E11 hearts are set as 1. Error bar: SEM.

d, RNA *in situ* analysis of *Mhrt* (blue) in adult hearts. The RNA probe targets all *Mhrt* species. Red: nuclear fast red. White arrowheads: myocardial nuclei. Black arrowheads: nuclei of endothelial, endocardial or epicardial cells. Dashed lines demarcate the myocardium from endocardium (endo) or from epicardium (epi). Scale= 50 μm.
e, RT-qPCR of nuclear/cytoplasmic RNA in adult hearts. *TfIIb*, *Hprt1*, and 28SrRNA are primarily cytoplasmic RNAs; *Neat1*, nuclear lncRNA. *TfIIb* ratio is set as 1. P-value: Student's t-test. Error bar: SEM.
f, Ribosome profiling: ribosome density on coding RNAs and lncRNAs.

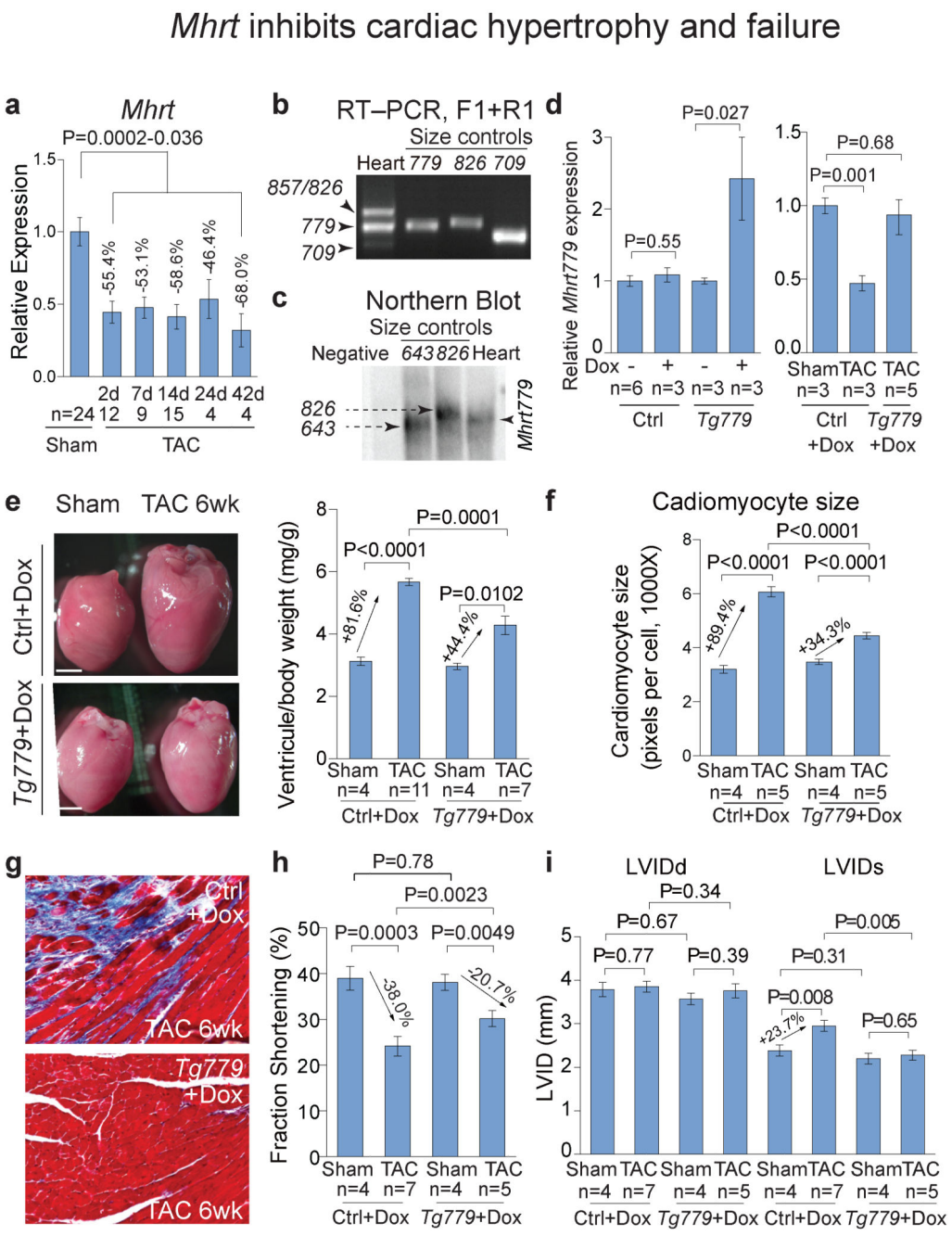

Figure 2. *Mhrt* inhibits cardiac hypertrophy and failure

a, Quantitation of cardiac *Mhrt*s 2–42 days after TAC operation. P-value: Student's t-test. Error bar: SEM.

b, RT-PCR of *Mhrts* in adult heart ventricles. Primers (F1 and R1, Fig. 1a) target *Mhrt* common regions. Size controls 779, 826, 709 are PCR products of recombinant *Mhrt779*, *Mhrt826*, and *Mhrt709*, respectively.

c, Northern blot of *Mhrts* in adult heart ventricles. The probe targets common regions of *Mhrts*. Negative: control RNA from 293T cells. Size control 826 is recombinant *Mhrt826*; 643 (not a distinct *Mhrt* species) contains the 5′ common region of *Mhrt*.

d Quantitation of *Mhrt779* in control or *Tg779* mice with/without doxycycline (Dox) or TAC operation. *Mhrt779*-specific PCR primers were used. Ctrl: control mice. *Tg779*: *Tnnt2-rtTA*;*Tre-Mhrt779* mice. P-value: Student's t-test. Error bar: standard error of the mean (SEM).

e, Ventricle-body weight ratio of hearts 6 weeks after TAC. P-value: Student's t-test. Error bar: SEM. Scale=1 mm.

f, Quantitation of cardiomyocyte size in control and *Tg779* mice 6 weeks after TAC by wheat-germ agglutinin staining. P-value: Student's t-test. Error bar: SEM.

g, Trichrome staining in control and *Tg779* hearts 6 weeks after TAC. Red: cardiomyocytes. Blue: fibrosis.

h, i, Echocardiographic measurement of left ventricular fractional shortening (**h**) and internal dimensions at end-diastole (LVIDd) and end-systole (LVIDs) (**i**) 6 weeks after TAC. P-value: Student's t-test. Error bar: SEM.

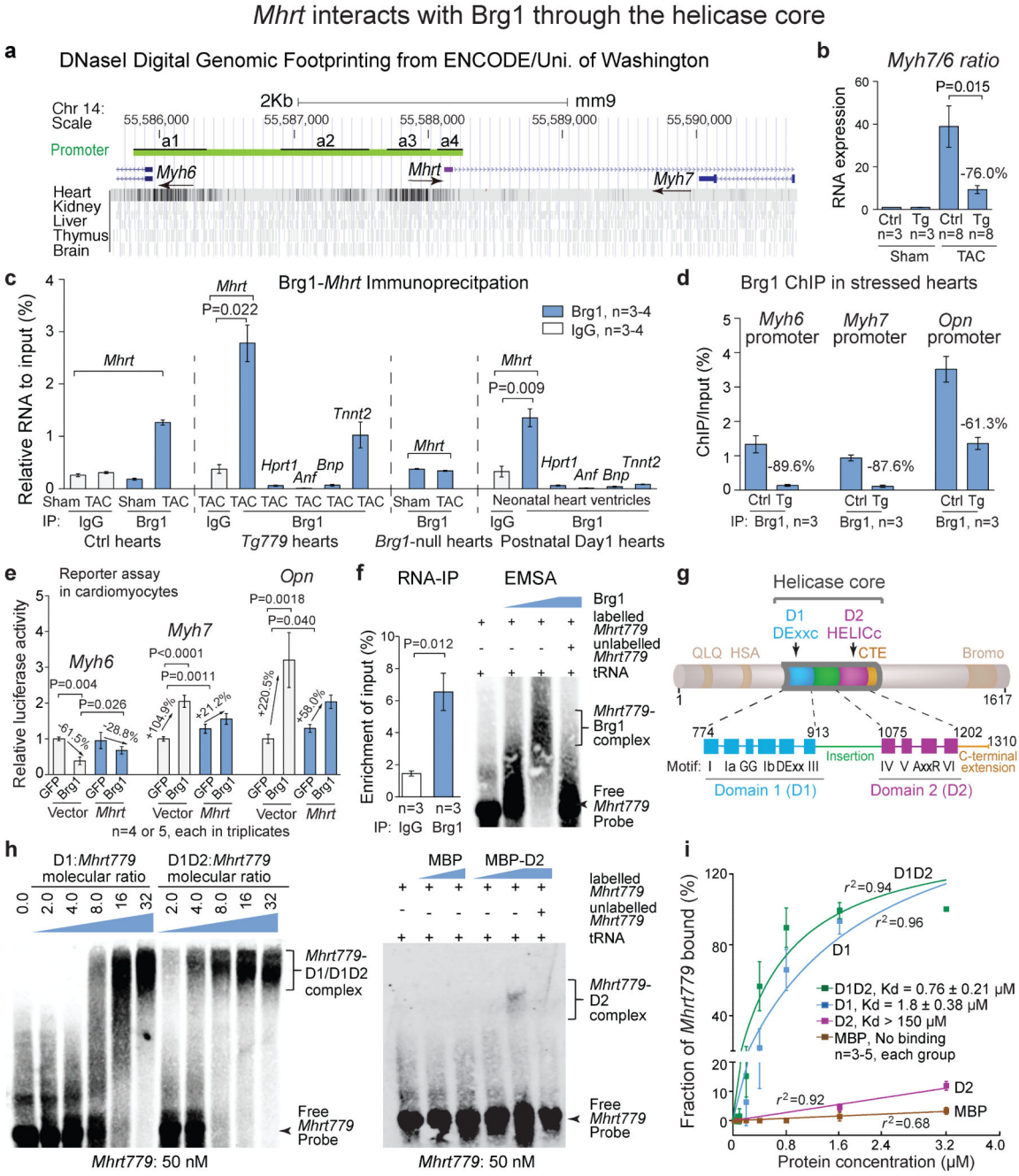

Figure 3. *Mhrt* complexes with Brg1 through the helicase domain

a, DNaseI digital footprinting of *Myh6/Mhrt* promoter loci from ENCODE. *Myh6* and *Mhrt* are transcribed in opposite directions as indicated by arrows. Bars represent DNA fragments protected from DNaseI digestion. Black boxes (a1-a4) refer to promoter regions with high sequences homology (Extended Data Fig. 4a).

b, Quantitation of *Myh7/Myh6* ratio in control (Ctrl) and *Tg779* (*Tg*) hearts 2 weeks after TAC. P-value: Student's t-test. Error bar: standard error of the mean (SEM).

c, RNA immunoprecipitation (RNA-IP) of *Mhrt*-Brg1 in ventricles from control hearts (Ctrl) with Sham/TAC operation; *Tg779* hearts after TAC; *Brg1*-null (*Tnnt2-rtTA;Tre-Cre;Brg1*$^{f/f}$) hearts after TAC; P1 hearts. P-value: Student's t-test. Error bar: SEM.

d, ChIP analysis of Brg1 in control (Ctrl) and *Tg779* hearts 2 weeks after TAC. Error bar: SEM.

e, Luciferase reporter assay of *Myh6* and *Myh7* promoters in neonatal rat cardiomyocytes. Vector: pAdd2 empty vector. *Mhrt*: pAdd2-*Mhrt779*. P-value: Student's t-test. Error bar: SEM.

f, RNA-IP and EMSA of recombinant Brg1 proteins and *in vitro* transcribed *Mhrt779*. Biotin-labeled *Mhrt779*: 50 nM; unlabeled *Mhrt779*: 500 nM. P-value: Student's t-test. Error bar: SEM.

g, Schematics of mouse Brg1 protein. The helicase core includes DExx-c and HELIC-c domain.

h, EMSA of *Mhrt779* and Brg1 helicase. MBP: maltose binding protein. MBP-D1: MBP fused to Brg1 D1 (aa 774–913). MBP-D2: MBP fused to Brg1 D2 (aa 1086–1310). MBP-D1D2: MBP fused to Brg1 D1D2 (aa 774–1310).

i, Binding affinity of *Mhrt779* for MBP-tagged D1D2 determined by EMSA. Error bars represent the standard error from multiple independent measurements. Nonlinear regression curves were generated by GraphPad Prism.

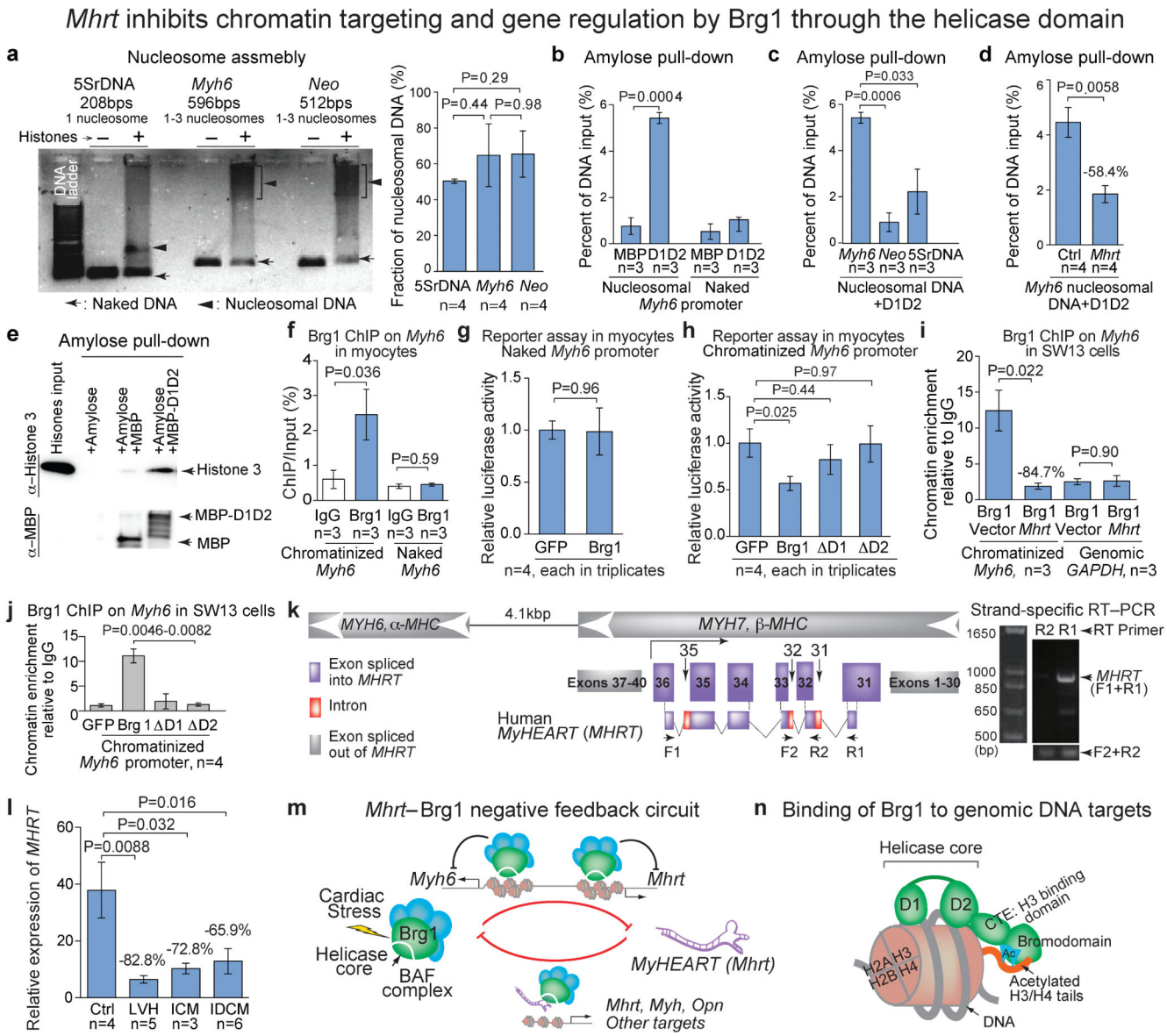

Figure 4. *Mhrt* inhibits chromatin targeting and gene regulation by Brg1

a, Gel electrophoresis and quantitation of nucleosomal 5SrDNA, *Myh6* promoter and *Neo* DNA. Arrowheads: DNA-histone complex. Arrows: naked DNA. Nucleosome assembly efficiency is defined as the fraction of DNA bound to histones (arrowheads). P-value: Student's t-test. Error bar: standard error of the mean (SEM).

b-d, Quantification of amylose pull-down of MBP-D1D2 (D1D2) with nucleosomal and naked *Myh6* promoter DNA (**b**), with nucleosomal *Myh6* promoter, *Neo*, and 5SrDNA (**c**), or with nucleosomal *Myh6* promoter in the presence of *Mhrt779* (**d**). P-value: Student's t-test. Error bar: SEM.

e, Amylose pull-down of MBP-D1D2 and histone 3. Anti-histone 3 and anti-MBP antibodies were used for western blot analysis.

f, ChIP analysis of Brg1 on chromatinized and naked *Myh6* promoter in rat ventricular cardiomyocytes. GFP: green fluorescence protein control. P-value: Student's t-test. Error bar: SEM.

g, h, Luciferase reporter activity of Brg1 on naked *Myh6* promoter (**g**) or of helicase-deficient Brg1 on chromatinized *Myh6* promoter (**h**) in rat ventricular cardiomyocytes. ΔD1: Brg1 lacking amino acid 774–913; ΔD2: Brg1 lacking 1086–1246. GFP: green fluorescence protein control. ChIP: H-10 antibody recognizing N-terminus, non-disrupted region of Brg1. P-value: Student's t-test. Error bar: SEM.

i, j, ChIP analysis in SW13 cells of chromatinized *Myh6* promoter in the presence of *Mhrt779* (**i**) or helicase-deficient Brg1 (**j**). Vector: pAdd2 empty vector. *Mhrt*: pAdd2-*Mhrt779*. P-value: Student's t-test. Error bar: SEM.

k, Schematic illustration and PCR of human *MHRT*. *MHRT* originates from *MYH7* and is transcribed into *MYH7*. *MYH7 e*xons and introns are indicated. R1 and R2 are strand-specific PCR primers; F1 and R1 target *MHRT* and *MYH7*; F2 and R2 are specific for *MHRT*.

l, Quantification of *MHRT* in human heart tissues. Ctrl: control. LVH: left ventricular hypertrophy. ICM: ischemic cardiomyopathy. IDCM: idiopathic dilated cardiomyopathy. P-value: Student's t-test. Error bar: SEM.

m, Working model of a Brg1-*Mhrt* negative feedback circuit in the heart. Brg1 represses *Mhrt* transcription, whereas *Mhrt* prevents Brg1 from recognizing its chromatin targets. Brg1 functions through two distinct promoter elements to bidirectionally repress *Myh6* and *Mhrt* expression.

n, Molecular model of how Brg1 binds to its genomic DNA targets. Brg1 helicase (D1D2) binds chromatinized DNA, C-terminal extension (CTE) binds histone 3 (H3), and bromodomain binds acetylated (Ac) histone 3 or 4 (H4).

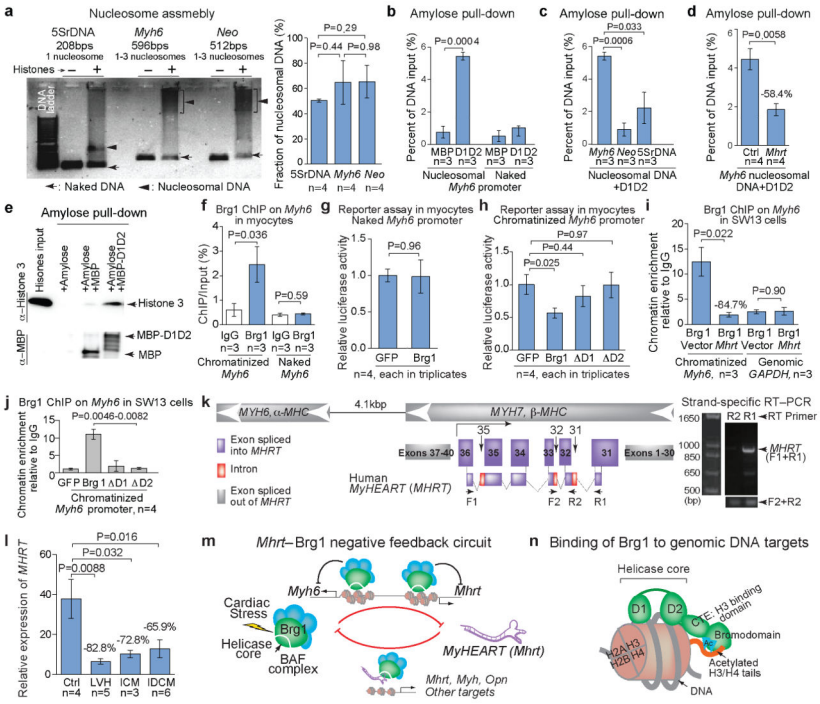

Figure 5.